

UC Riverside

UC Riverside Previously Published Works

Title

Chemical Composition and Optical Properties of Secondary Organic Aerosol from Photooxidation of Volatile Organic Compound Mixtures.

Permalink

<https://escholarship.org/uc/item/54p801rr>

Authors

Cui, Yumeng

Chen, Kunpeng

Zhang, Haofei

et al.

Publication Date

2024-04-12

DOI

10.1021/acsestair.3c00041

Peer reviewed

Chemical Composition and Optical Properties of Secondary Organic Aerosol from Photooxidation of Volatile Organic Compound Mixtures

Yumeng Cui, Kunpeng Chen, Haofei Zhang, Ying-Hsuan Lin, and Roya Bahreini*



Cite This: *ACS EST Air* 2024, 1, 247–258



Read Online

ACCESS |

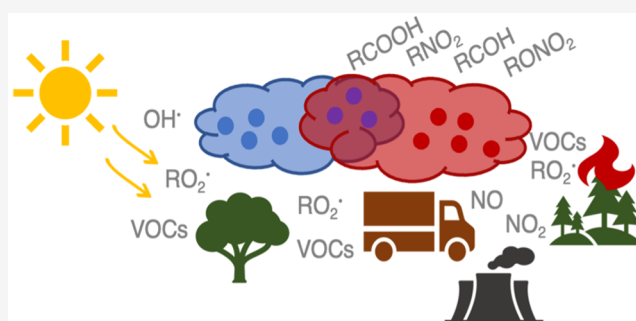
Metrics & More

Article Recommendations

Supporting Information

ABSTRACT: The chemical and optical properties of secondary organic aerosols (SOA) have been widely studied through environmental chamber experiments, and some of the results have been parametrized in atmospheric models to help understand their radiative effects and climate influence. While most chamber studies investigate the aerosol formed from a single volatile organic compound (VOC), the potential interactions between reactive intermediates derived from VOC mixtures are not well understood. In this study, we investigated the SOA formed from pure and mixtures of anthropogenic (phenol and 1-methylnaphthalene) and/or biogenic (longifolene) VOCs using continuous-flow, high- NO_x photooxidation chamber experiments to better mimic ambient conditions. SOA optical properties, including single scattering albedo (SSA), mass absorption coefficient (MAC), and refractive index (RI) at 375 nm, and chemical composition, including the formation of oxygenated organic compounds, organic-nitrogen compounds (including organonitrates and nitro-organics), and the molecular structure of the major chromophores, were explored. Additionally, the imaginary refractive index values of SOA in the multi-VOC system were predicted using a linear-combination assumption and compared with the measured values. When two VOCs were oxidized simultaneously, we found evidence for changes in SOA chemical composition compared to SOA formed from single-VOC systems, and this change led to nonlinear effects on SOA optical properties. The nonlinear effects were found to vary between different systems.

KEYWORDS: secondary brown carbon, multi-VOC systems, SOA optical properties, SOA chemical composition, nitro-aromatic compounds



1. INTRODUCTION

Aerosols' radiative forcing has been studied extensively over the past decades, as aerosols directly and indirectly influence the Earth's radiative budget and climate.^{1–4} However, the understanding of the chemical and optical properties of organic aerosols (OA) is still incomplete, influencing the modeled aerosol global and regional climate forcings.^{5–8} Traditionally, OA were recognized as scattering species, which scatter the solar radiation and lead to a cooling effect of the surrounding air; however, with more studies investigating the optical properties of both lab-generated and ambient aerosols, some OA show varying degrees of absorption within visible (Vis) and ultraviolet (UV) wavelengths. This subclass of OA with a strong wavelength-dependence of absorption are defined as brown carbon (BrC) aerosols.^{1,3,9–11}

Biomass burning and smoldering combustion produce BrC aerosols directly.^{1,2,10,11} Additionally, BrC can also be generated from atmospheric oxidation reactions of volatile organic compounds (VOCs) and different oxidants, and they are classified as secondary BrC aerosols or light-absorbing secondary organic aerosols (SOA).^{3,9,12} Previous studies

proved that the absorption of these secondary BrC aerosols can be enhanced under certain conditions, including in the presence of NO_x , NH_3 , or higher relative humidity.^{9,12–15} Particularly, aromatic SOA show higher absorption that is close to the absorption of aerosols in near-source biomass burning plumes in the presence of NO_x .^{9,12,15–18} Chemical characterization of the SOA indicates that nitrogen-containing aromatic compounds, polycyclic aromatic hydrocarbons (PAH), and phenolic compounds are among the commonly seen chromophores in BrC aerosols.^{11,15,19–21} However, since our current understanding of light-absorbing OA is insufficient to accurately describe measured ambient OA absorption,^{6,8} more

Received: September 22, 2023

Revised: February 14, 2024

Accepted: February 14, 2024

Published: February 29, 2024



Table 1. Summary of the Experiments

VOC ^a	[VOC] ₀ ^b (ppbv)	initial OH reactivity ^c (s ⁻¹)	[NO] ₀ /[NO ₂] ₀ ^d (ppbv)	RI ^e		[M _{OA}] ^g (μg/m ³)	plot reference
				n ₃₇₅ /k ₃₇₅	MAC _{org} ^f (m ² /g)		
phenol	95	60	470/160	1.75/0.080	3.58	80	I
phenol	85	55	520/120	1.72/0.068	2.93	130	II
MN	50	50	580/85	1.51/0.018	0.56	70	III
MN	75	75	560/75	1.43/0.014	0.52	105	IV
Lgf	25	30	650/100	1.45/0.001	0.06	220	V
Lgf	20	25	710/45	1.49/0.001	0.09	160	VI
Ph+Lgf	105 + 115	70 + 135	555/105	1.57/0.022	1.50	510	VII
Ph+Lgf	100 + 75	65 + 90	490/60	1.56/0.024	1.55	500	VIII
Ph+Lgf	100 + 95	65 + 110	665/95	1.57/0.021	1.47	300	IX
Ph+Lgf	85 + 30	55 + 35	610/30	1.52/0.029	1.61	200	X
MN+Lgf	45 + 30	45 + 35	535/40	1.51/0.005	0.27	340	XI
MN+Lgf	40 + 15	40 + 20	615/40	1.60/0.006	0.25	300	XII
MN+Lgf	90 + 35	90 + 40	620/60	1.50/0.006	0.36	240	XIII
MN+Lgf	65 + 15	65 + 20	575/60	1.49/0.008	0.33	270	XIV

^aNote: Ph = phenol, MN = 1-methylnaphthalene, Lgf = longifolene. ^b[VOC]₀ is the VOC concentration based on GC-FID measurement at the beginning of each experiment. ^cInitial OH reactivity is calculated based on initial VOC concentration and the reaction rate constant between each VOC and OH[•]. Here, we controlled the injected VOC concentrations to have the initial OH reactivities of two VOCs in multi-VOC experiments stay at similar magnitudes. ^d[NO]₀/[NO₂]₀ are the concentrations of NO and NO₂ accordingly at the beginning of each experiment. ^eRI is the average derived refractive index values of SOA particles after 60 min reaction time. ^fMAC_{org} is the average SOA MAC values after 60 min reaction time. ^g[M_{OA}] is the organic aerosol peak mass concentration (not corrected for wall loss) during each experiment. For multi-VOC experiments VII–X and XI–XIV, the resulting SOA chemical and optical properties are highly similar. For the simplicity of the plots, data from experiments IX–X and XIII–XIV are not shown in Figures 1 and 2.

studies on SOA from various VOCs and in different aging environments are needed.

In addition to the need for understanding OA's absorption, it is critical to study SOA formation from multiple VOCs instead of a single VOC. Most of the current chamber and flow oxidation reactor experiments study the SOA formation from single VOC oxidation,^{12,19,20,22} while in the real ambient atmosphere, as one can imagine, multiple VOCs from different sources mix and react with other reactive species to form SOA that may be different from the SOA from a single-VOC system.^{23–25} McFiggans et al. found that with α -pinene and isoprene present in one system, isoprene would scavenge the OH radicals (OH[•]) and reduce the formation of oxygenated α -pinene products, thus eventually reducing the contribution of α -pinene SOA in the mixture.²⁶ In a more recent study, Takeuchi et al. shows that the SOA yield in a system consisting of two monoterpenes changed compared to any single-monoterpene system, and this change was accompanied by the change in aerosol chemical composition and volatility.²⁷ These nonlinear effects have also been observed in SOA optical properties in multi-VOC systems.⁹ However, the authors did not elucidate the cause of the absorption enhancement and reduction due to the lack of detailed chemical molecular measurements.

In this study, we investigated the formation of BrC SOA in single- vs multi-VOC systems and compared their chemical composition and optical properties. Specifically, we studied the SOA formation from systems of: pure phenol, 1-methylnaphthalene, longifolene, and the mixtures of phenol + longifolene and 1-methylnaphthalene + longifolene. Phenol and 1-methylnaphthalene, commonly found in urban and wildfire emission sources, are selected because of their potential in producing light-absorbing SOA, while longifolene, a biogenic VOC with high SOA formation yield, has been shown to mainly produce light-scattering SOA.^{14,16,22} Aerosol chemical composition (measured by mass spectrometry) was used to

evaluate the influencing factors of the observed variation in aerosol absorption in different systems. Additionally, the imaginary component of refractive index of the multi-VOC SOA was predicted based on a source apportionment model and was compared with the measured values.

2. METHODS

2.1. Chamber Experiments and Online Measurements.

The experiments were carried out in a 1.5 m³ PFA Teflon chamber bag enclosed in a metallic frame. A more detailed description of the chamber setup can be found in Dingle et al. and Cui et al.^{14,16} The chamber bag was first filled with zero grade air (Airgas, $\geq 99.8\%$), and then 100 μ L of H₂O₂ solution (Sigma-Aldrich, 50 wt % in H₂O) and VOC (phenol, Sigma-Aldrich, $\geq 99.0\%$; 1-methylnaphthalene, Sigma-Aldrich, 95%; longifolene, MP Biomedicals, 91.9%) were injected into the chamber bag with a gentle flow of zero grade air and gentle heating through a glass manifold. Additionally, high concentration of NO (Airgas, 495 ppm in nitrogen) was injected into the bag to achieve the initial NO concentration above 450 ppbv. After the gas-phase VOC and NO_x concentrations were stabilized, the UV lights (Sylvania black lights, 350 nm) were turned on. To have continuous OH[•] production, another 50 μ L of H₂O₂ was injected into the chamber with a gentle flow of zero-grade air (1–2 L/min¹) over 60–100 min. The resulting average OH[•] concentration in the chamber bag, estimated in a separate experiment by monitoring the decay of octane, was determined to be about 1.1×10^7 molecules/cm³. Additionally, NO was injected periodically during the experiment to maintain the NO concentration in the bag above 350 ppbv, while NO was continuously oxidized to NO₂ in the chamber. On average, the total amount of NO injected into the bag during a 2.5 h experiment was about 6.8–7.1 L of the NO mixture (495 ppm in N₂). The experiments were done under dry conditions (relative humidity <10%) and room temperature (22–25 °C).

Table 1 shows a summary of the experimental conditions discussed in this work.

Upon irradiation of the mixture with UV, SOA particles were produced from nucleation and condensation and monitored by different instruments. The maximum mass concentrations (without wall-loss correction) from chamber experiments were about 70–500 $\mu\text{g}/\text{m}^3$, depending on the VOC precursors and concentrations. In this work, a set of instruments was used to study both gas- and particle-phase compounds. The gas-phase instruments include a gas chromatograph coupled with a flame ionizing detector (GC-FID, Hewlett Packard 5890 Series II) to monitor the VOC concentration in the bag; a UV photometric ozone analyzer (Thermo, model 49i), and a chemiluminescence NO–NO₂–NO_x analyzer (Thermo, model 42i) to measure the gas phase ozone and NO–NO₂–NO_x concentrations, respectively.

For particle-phase measurements, the air from the chamber bag was sampled by various instruments through a 30 cm long purifier containing Purafil (Thermo Scientific). A scanning electrical mobility spectrometer (SEMS, Brechtel Manufacturing Inc.) was used to measure the aerosol particle number concentration and size distribution in the range 10–740 nm during a 140 s scan, and the particle volume concentration was integrated from these values. The accuracy of the SEMS size measurement was determined as $\pm 4\%$ based on calibrations with polystyrene latex sphere standards. Aerosol particles' absorption and scattering coefficients at 375 nm ($\beta_{\text{abs},375}$ and $\beta_{\text{scat},375}$) were measured by a photoacoustic extinctionsmeter (PAX, Droplet Measurement Technology) at 1 Hz. $\beta_{\text{abs},375}$ and $\beta_{\text{scat},375}$ were then averaged to the SEMS time (140 s); $\beta_{\text{abs},375}$ and $\beta_{\text{scat},375}$ detection limits were defined as two times the standard deviation of the averaged values during internal filtered-air sampling and were 0.93 and 1.11 Mm^{-1} , respectively. A mini-aerosol mass spectrometer (mAMS, Aerodyne Research, Inc.) was used to measure size-resolved aerosol particles chemical composition. Since particles nucleated fast at the beginning of the photooxidation reaction, the relatively long sample time of SEMS could not track the particle growth very well during this initial period; thus, in the following sections we only discuss the results when the mode of the size distribution increased by less than 10% between two consecutive SEMS runs.

2.2. Offline Measurements. Aerosol particles were collected onto polytetrafluoroethylene membrane filters (Whatman, 47 mm, 1.0 μm pore size) after 2–2.5 h of photooxidation. The filter samples were stored at $-20\text{ }^\circ\text{C}$ immediately after collection to avoid the loss of semivolatile compounds. Before analyzing with offline instruments, the filter samples were extracted with 22 mL of acetonitrile (Fisher Scientific, HPLC grade) by 50 min sonication. The extracted solution was then dried with a gentle flow of nitrogen ($\geq 99.8\%$, Airgas). Finally, the residues were reconstituted in 100 μL of acetonitrile for measurements by an ultra-performance liquid chromatography (UPLC) coupled with a diode array detector (DAD), and a high-resolution quadrupole time-of-flight mass spectrometer equipped with an electrospray ionization source (ESI-HR-QTOFMS, Agilent 6545 series). The ESI was operated in negative ion mode. This instrument chromatographically separates the different components of the sample and then characterizes its molecular composition and the corresponding absorbance at the same time, thus allowing us to identify the molecular formula of the absorbing species in the extracted SOA particles as well as the wavelength-

dependent SOA absorbance. The technical details can be found in previous studies and SI.^{28,29}

2.3. Optical Characterization. To discuss and compare the absorption by SOA particles from different systems, particles' single scattering albedo (SSA), mass absorption coefficient (MAC), and refractive index (RI) were calculated and derived in all the experiments. SSA and MAC at 375 nm were calculated as follows:

$$\text{SSA}_{375} = \frac{\beta_{\text{scat},375}}{\beta_{\text{scat},375} + \beta_{\text{abs},375}} \quad (1)$$

$$\text{MAC}_{375} = \frac{\beta_{\text{abs},375}}{M_{\text{OA}}} \quad (2)$$

where M_{OA} is the mass concentration of SOA in each system. More details of the calculations can be found in Cui et al.¹⁴ Particles' SSA is size-dependent; thus, we display SSA as a function of particle size parameter at $\lambda = 375\text{ nm}$ (α_{375} , defined in eq 3, d_m refers to the aerosol electrical mobility diameter) in the following sections. The relative uncertainties in SSA_{375} and MAC_{375} were determined from propagating errors in $\beta_{\text{scat},375}$, $\beta_{\text{abs},375}$, and M_{OA} , and they were 6% and 25%, respectively.

$$\alpha_{375} = \frac{\pi d_m}{\lambda} \quad (3)$$

RI values indicate the interaction between aerosol particle material and radiation with the real part (n) indicating the scattering properties of the particle and the imaginary part (k) indicating the absorbing properties. The derivation of RI values of the aerosol particles was based on Mie theory and an optical closure procedure described previously.^{30–32} Generally, theoretical $\beta_{\text{scat},375}$ and $\beta_{\text{abs},375}$ were calculated with pre-assumed n and k and SMES-measured particle size distributions. The overall, final n_{375} and k_{375} of the particles were determined by comparing the calculated and measured $\beta_{\text{scat},375}$ and $\beta_{\text{abs},375}$ until a deviation merit function χ^2 was minimized:

$$\chi^2 = \frac{(\beta_{\text{scat,meas}} - \beta_{\text{scat,calc}})^2}{\varepsilon_{\text{scat,meas}}^2} + \frac{(\beta_{\text{abs,meas}} - \beta_{\text{abs,calc}})^2}{\varepsilon_{\text{abs,meas}}^2} \quad (4)$$

where, $\beta_{\text{scat,meas}}$ and $\beta_{\text{abs,meas}}$ are the averaged 1 Hz optical coefficients during the 140 s sampling time of SEMS, $\varepsilon_{\text{meas}}$ is the standard deviation of the corresponding averaged optical data, and $\beta_{\text{scat,calc}}$ and $\beta_{\text{abs,calc}}$ are the calculated optical coefficients. The refractive index values of the SOA were estimated based on the SOA volume fraction of the aerosols and the calculated overall refractive index. Details of the calculation can be found in previous studies.^{16,33}

2.4. Online Chemical Characterization. Although the high vaporization temperature and ionization energy of mAMS fragment the particles into ions with relatively small mass-to-charge ratios (m/z), we can still rely on some ions to study the oxidation and aging status and functional group formation of aerosol particles. All experiments in this work were done under high-NO_x conditions with OH* as the oxidant; thus, we expect the formation of oxygenated organic compounds, organonitrate, and nitro-organic compounds in the SOA particles. The studied organic and nitrogen-containing ions and families include $m/z = 43$ ($\text{C}_2\text{H}_3\text{O}^+$), $m/z = 44$ (CO_2^+), $m/z = 30$ (NO^+), $m/z = 46$ (NO_2^+), family CHN^+ , family CHO_1N^+ , and family $\text{CHO}_{>1}\text{N}^+$.

Mass concentrations and fractions of $m/z = 43$ ($C_2H_3O^+$) and $m/z = 44$ (CO_2^+) indicate the presence of oxygenated compounds in the particle-phase, with $C_2H_3O^+$ being a major ion from carbonyl compounds and CO_2^+ a major ion from fragmentation of carboxylic acid, peroxide, hydroperoxide, and ester compounds.³⁴ Fractional contributions of $C_2H_3O^+$ and CO_2^+ to total organics ($F_{C_2H_3O}$, F_{CO_2}) were calculated (see details in SI).

The ratio of $m/z = 30$ (NO^+) to $m/z = 46$ (NO_2^+) indicates the formation of particle-phase organic-nitrogen compounds (ON, including organonitrates and nitro-organics) due to the difference in fragmentation patterns between ON and inorganic nitrate.^{35,36} The mass fraction of ON functional groups to total organics (F_{ON}) was calculated following the procedure highlighted in Day et al. (see details in the SI).³⁶ In addition, the formation of nitro-organic compounds could lead to the formation of fragment ions such as CHN^+ , CHO_1N^+ , and $CHO_{>1}N^+$ families in mAMS. Therefore, we also calculated the sum of mass concentrations of these three nitrogen-containing organic families and their fractions in total organics ($F_{N-family}$; see details in the SI). Thus, F_{ON} indicates the formation of both organonitrates and nitro-organics, while the $F_{N-family}$ value is more of an indicator for the formation of nitro-organics.

2.5. Source Apportionment Model and k Prediction.

In this work, we conducted experiments with both single-VOC and multi-VOC systems and compared the absorbing properties of the SOA particles from the two systems. We hypothesized that, in the multi-VOC system, unique compounds may be formed that were not observed in the single-VOC system, and these compounds may influence the final k_{375} of the multi-VOC SOA. To test this hypothesis, we estimated the contribution of SOA from each VOC in the mixture SOA following two methods. First, we used a source apportionment tool (*SoFi 6.F2*)³⁷ that utilized the mAMS mass spectra of SOA particles from single-VOC systems to estimate the contribution of this SOA in the multi-VOC system throughout the experiments. The uncertainty in the factor contributions was determined to be 2–10.5% following the method outlined in Lin et al.^{38,39} In the second method, we estimated the SOA mass formed from each VOC using the SOA yield values in literature^{22,40,41} and the reacted concentrations of the VOCs. In either method, by assuming that the multi-VOC SOA was made of two types of SOA from the single-VOC experiments, we obtained the fraction of each component in the multi-VOC SOA ($Frac_{aromatic}$ and $Frac_{lgf}$). We then predicted the k value of the multi-VOC SOA ($k_{375,prd}$) using these fractions and the corresponding k_{375} values from single-VOC experiments (eq 5). $k_{375,prd}$ was then compared with $k_{375,meas}$ in the multi-VOC experiments. Additional details are listed in section 3.3 and the SI.

$$k_{375,prd} = k_{375,aromatic} \times Frac_{aromatic} + k_{375,Lgf} \times Frac_{Lgf} \quad (5)$$

3. RESULTS AND DISCUSSION

3.1. Optical and Chemical Properties of SOA from Single-VOC Systems.

The different VOCs (phenol, 1-methylnaphthalene, and longifolene) studied in this work showed different nucleation and growth properties in the experiments. Particles nucleated and grew fastest in longifolene experiments, and the particle volume concentration reached

peak values after 50–60 min of oxidation. On the other hand, nucleation was slower in phenol and 1-methylnaphthalene experiments, and particle number concentration reached peak values after 70–80 min of oxidation. The longifolene particles grew to a larger size (250–290 nm) compared to aromatic particles (phenol: 230 nm; 1-methylnaphthalene: 110 nm).

In addition to particle growth, the SOA observed from these VOCs also showed different optical and chemical properties (shown in Figures 1 and 2 and Figure S11). Below, we discuss the experimental results in two groups.

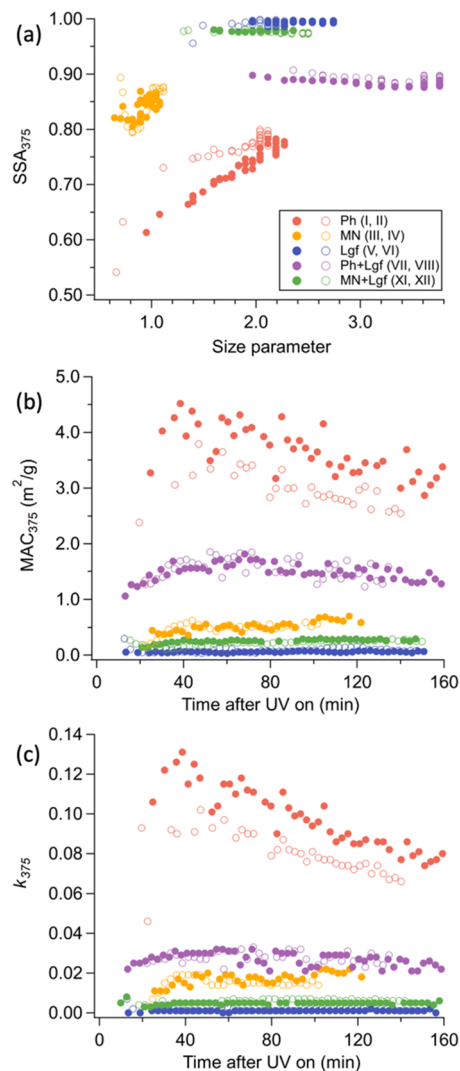


Figure 1. (a) SSA_{375} vs size parameter at 375 nm, (b) MAC_{375} , and (c) k_{375} vs reaction time of SOA particles from five different systems. The open and closed markers represent the duplicate experiments.

3.1.1. Aromatic VOC systems.

Despite both being aromatic VOCs, phenol and 1-methylnaphthalene SOA showed different degrees of absorbing properties (phenol: $SSA_{375} = 0.76$, $MAC_{375} = 3.30 \text{ m}^2/\text{g}$, $k_{375} = 0.074$; 1-methylnaphthalene: $SSA_{375} = 0.85$, $MAC_{375} = 0.54 \text{ m}^2/\text{g}$, and $k_{375} = 0.016$), as shown in Figure 1. The measured MAC_{375} of the aromatic SOA is comparable to or higher than the MAC of other aromatic and biomass burning SOA in previous literature, suggesting the formation of chromophores in both phenol and 1-methylnaphthalene SOA. For example, here are values of some measured MAC at near-UV range in recent light-

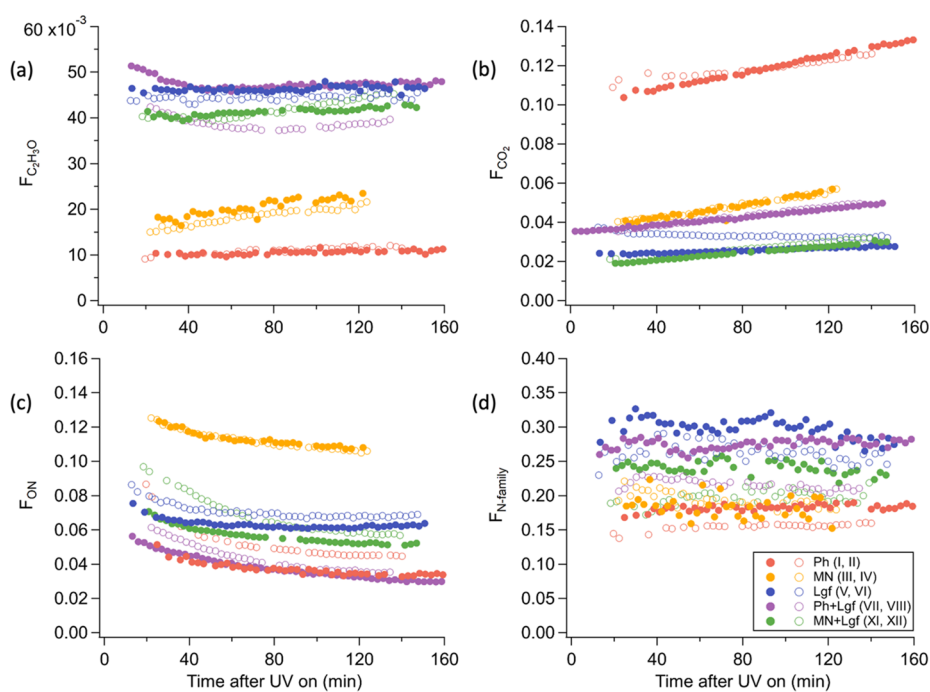


Figure 2. Calculated (a) $F_{C_2H_3O^+}$, (b) $F_{CO_2^+}$, (c) F_{ON^+} , and (d) $F_{N\text{-family}}$ of SOA particles from five different systems.

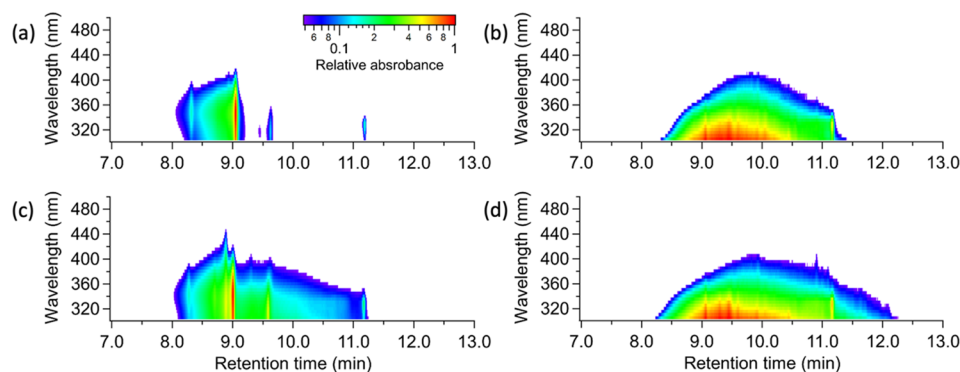


Figure 3. UPLC-DAD chromatograms (in negative mode) of (a) phenol, (b) 1-methylnaphthalene, (c) phenol + longifolene, and (d) 1-methylnaphthalene + longifolene samples. The *x*-axis is the UPLC retention time, and the *y*-axis is the DAD wavelength. Relative absorption intensity is color-coded, as shown in the legend.

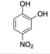
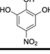
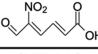
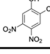

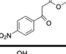
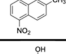

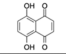
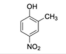
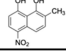
absorbing SOA studies: $MAC \approx 0.2\text{--}1.5 \text{ m}^2/\text{g}$ near 370 nm;⁴² $MAC \approx 0.6\text{--}1.2 \text{ m}^2/\text{g}$ near 370 nm;¹² $MAC \approx 0.05\text{--}1.2 \text{ m}^2/\text{g}$ near 370 nm.¹⁵ Phenolic compounds have been identified as important products and chromophores in biomass burning emissions,^{11,43,44} and some studies have explored the formation of phenol SOA BrC from aqueous and gas-phase oxidation reactions.^{16,45–47} Our experimental results confirmed the formation of highly absorbing compounds from phenol photooxidation under high NO_x conditions. Furthermore, the observed MAC_{375} and k_{375} for phenol SOA were even higher than some of those measured in biomass burning emissions.^{42,43,48} Interestingly, MAC_{375} of phenol SOA decreased with experimental time, indicating that at the beginning of the oxidation reactions, absorbing molecules formed fast, while upon further oxidation, either the chromophore formation slowed down or the chromophores were “diluted” by condensation of compounds that were more scattering in nature.⁹

Based on results from our previous experiments, in high- NO_x batch photooxidation experiments, MAC_{375} of 1-

methylnaphthalene SOA reached $0.4 \text{ m}^2/\text{g}$ after 120 min of oxidation,¹⁴ while in the current continuous-flow experiments, the corresponding value was about $0.6 \text{ m}^2/\text{g}$, indicating that either the presence of continuous flow of OH^* or NO (and subsequently continuous formation of NO_2) increased the final SOA MAC_{375} . Considering the average OH^* concentration in the two types of experiments ($3.6 \times 10^7 \text{ molecules}/\text{cm}^3$ in batch experiments vs. $1.1 \times 10^7 \text{ molecules}/\text{cm}^3$ in continuous-flow experiments), NO_x concentration was more likely to be the reason for higher MAC_{375} .

To explore the chemical functional groups that influenced BrC formation, we compared the chemical characteristics of SOA in different experiments (Figure 2). Among the markers of oxidized products, phenol and 1-methylnaphthalene SOA showed a lower $C_2H_3O^+$ fraction but a higher CO_2^+ fraction compared to longifolene SOA, suggesting that both aromatic VOCs have gone through significant oxidation reactions and have formed more oxidized products with low vapor pressure, especially in phenol experiments since the fractions of highly oxidized compounds were much higher than the rest of the

Table 2. Molecular Characteristics of Chromophores Identified in Phenol, Ph+Lgf, MN, and MN+Lgf SOA Samples from UPLC-DAD-ESI-HR-QTOFMS Measurements

^a In system	^b Retention time (min)	Measured m/z (H)	^c Proposed structure/formula
Phenol, Ph+Lgf	8.3, 9.0, 9.3, 9.6, 11.1	154	
Phenol, Ph+Lgf	8.3	170	
Phenol, Ph+Lgf	8.9	140	C ₅ H ₃ NO ₄ /C ₆ H ₇ NO ₃
Phenol, Ph+Lgf	9.0	171	
Phenol, Ph+Lgf	9.0	124	C ₆ H ₇ NO ₂
Phenol, Ph+Lgf	9.3, 9.6	199	
Phenol, Ph+Lgf	9.3, 9.6	138	
Phenol, Ph+Lgf	9.6	108	CH ₃ NO ₅ /C ₆ H ₇ NO
Phenol	9.6	242	C ₁₃ H ₂₅ NO ₃
Phenol	11.1	236	
MN, MN+Lgf	9.0-11.1	202	
MN, MN+Lgf	9.0, 9.4	138	
MN, MN+Lgf	9.0, 9.3, 9.4	119	C ₂ H ₄ N ₂ O ₄
MN, MN+Lgf	9.4, 9.6	189	
MN, MN+Lgf	9.6, 9.9	223	C ₉ H ₆ NO ₄
MN, MN+Lgf	9.9	152	
MN, MN+Lgf	11.1	218	

^a“In system” represents in which sample we have found the corresponding chemical ions. ^b“Retention time” represents the retention time of the corresponding chemical ions. The isomers of each compound may elute at different retention times. ^c“Proposed structure/formula” are assigned based on accurate mass measurements and literature reports.

studied SOA. 1-Methylnaphthalene SOA displayed a much higher fraction of ON than other SOA, while phenol SOA showed almost the lowest fraction of ON. With the presence of NO₂, high fractions of nitrogen-containing organic ions were also observed in all experiments. These ions, believed to be from fragmentation of nitro-organic compounds, showed similar values in phenol and 1-methylnaphthalene experiments. With these observations, we infer that both phenol and 1-methylnaphthalene reacted with OH[•] and O₂ to produce R[•] and RO[•], which subsequently reacted with NO₂ and formed nitro-organic compounds; on the other hand, phenol RO₂[•] was more likely to form carboxylic acid, while 1-methylnaphthalene RO₂[•] was more likely to react with NO and form organo-nitrates.

Previous laboratory studies show that nitro-aromatic compounds like nitro-phenol and nitro-catechol contribute significantly to aromatic SOA absorption under high-NO_x conditions.^{15,42,44,47,49} Additionally, nitro-aromatics are also commonly found in biomass burning BrC aerosols. In this study, we proposed that nitro-aromatic compounds were the main chromophores in the two aromatic SOA systems. To relate the SOA chemical composition with its absorption, we proposed the molecular formula and/or structure of compounds with high absorbance from UPLC-DAD-ESI-HR-QTOFMS scanning. Figure 3a,b presents the UPLC-DAD chromatograms of phenol and 1-methylnaphthalene SOA samples, showing the presence of absorbing BrC chromo-

phores in both samples eluting at different retention times. Furthermore, using estimates of the Absorption Ångström Exponent (AAE) in the range of 375–425 nm based on the DAD background-subtracted absorbance measurements, we calculated *k* at 425 nm (*k*₄₂₅) for phenol (*k*₄₂₅ = 0.0023) and 1-methylnaphthalene SOA (*k*₄₂₅ = 7.4 × 10⁻⁵). The significantly higher *k*₄₂₅ for phenol SOA suggests presence of chromophores in these samples that strongly absorb strongly from the UV to the visible wavelength range (>400 nm), while the chromophores in 1-methylnaphthalene SOA samples only showed strong absorbance in the near UV wavelength range. The details of the calculations can be found in the SI. This explains our observation that the phenol SOA filter samples and the extracted solution showed yellow-brown colors. Due to the complex composition of SOA, it is challenging to elucidate and identify all BrC species, especially if some components co-eluted.²¹ Here, we focused on identifying some major chromophore species that were absorbing in near UV to visible wavelengths under negative ionization mode. Our results (shown in Table 2) indicated that nitro-aromatic products were the main detected light-absorbing components in both phenol and 1-methylnaphthalene SOA samples. Similar nitro-aromatic compounds were also identified as significant BrC chromophores in toluene and naphthalene photooxidation SOA samples formed under high-NO_x conditions,^{12,21,50} and in nitrate-radical initiated phenol oxidation SOA sample.⁴⁷ Siemens et al. found that, in addition to nitro-aromatics,

oxygenated aromatic compounds with hydroxyl, carboxyl, methyl, and aldehyde functional groups also contributed significantly to naphthalene photooxidation SOA under both low- and high-NO_x conditions.²¹ Our mAMS result confirmed the formation of these oxygenated compounds (C₂H₃O⁺ and CO₂⁺) in both aromatic SOA, especially the fraction of CO₂⁺ in phenol SOA was high and comparable with the fraction of nitro-organic compounds. However, based on the UPLC-DAD-ESI-HR-QTOFMS scanning results, most of the oxygenated products that were identified also have a nitro functional group. We believe this is due to the fact that aromatic compounds with nitro groups have higher electrospray ionization efficiencies and are preferentially detected by UPLC-DAD-ESI-HR-QTOFMS under negative ion mode,⁵¹ or because of the continuous flow of NO injected into the chamber bag, some of our oxygen-containing organic compounds were eventually converted to compounds with both nitro and oxygenated functional groups. Based on the current results, we infer that aromatic compounds with nitro and/or oxygenated functional groups contributed to the resulting SOA absorption in our systems. Additionally, although we confirmed the formation of nitro-aromatic compounds in both aromatic SOA and their $F_{N\text{-family}}$ values were close, their MAC₃₇₅ values varied a lot, so we infer that the content of nitro-organic compounds alone does not directly affect aromatic SOA absorption. In fact, it is the conjugated carbon backbone along with the nitro functional group that determines whether a molecule is absorbing or not.

3.1.2. Biogenic VOC System. Longifolene SOA was mostly light-scattering, with average SSA₃₇₅ around 0.99, MAC₃₇₅ less than 0.1 m²/g and k_{375} around 0.001. The lack of extended conjugated bonds in longifolene is believed to be the cause of the low absorption of its oxidation products.⁵² Longifolene SOA showed the highest fraction of C₂H₃O⁺ with the lowest CO₂⁺ fraction among all of the studied SOA, indicating the relatively lower extent of oxidation in its SOA products. Longifolene SOA showed a slightly higher fraction of ON compared to most of the studied SOA in this work. Longifolene SOA also contained a slightly higher fraction of nitro-organics compared to phenol and 1-methylnaphthalene SOA, indicating that longifolene radicals tended to form carbonyls, organonitrates, and/or nitro-organics instead of carboxylic acid, peroxide, hydroperoxide, or ester as stable products, and the nitro-organic groups that were not attached to the aromatic backbone did not absorb radiation at 375 nm. The UPLC-DAD chromatogram of the longifolene sample did not show any absorbance within the near UV-visible wavelengths, indicating the acetonitrile extractable SOA compounds were mostly scattering, which is consistent with the online optical measurement.

3.2. Optical and Chemical Properties of SOA from Multi-VOC Systems. A significant amount of SOA particles was observed in both multi-VOC systems. The addition of longifolene VOC with a relatively high SOA formation yield²² enhanced particle growth, with larger particle sizes being observed in the multi-VOC systems compared to the pure aromatic VOC systems (Figures S11 and S12). Below, we discuss the optical and chemical properties of SOA particles from the two different systems.

3.2.1. Phenol + Longifolene System. The SOA particles formed in the phenol + longifolene experiment were less absorbing than pure phenol SOA but more absorbing than pure longifolene SOA (phenol + longifolene: SSA₃₇₅ = 0.88,

MAC₃₇₅ = 1.52 m²/g, and k_{375} = 0.024). Consistent with the observations by Liu et al., the values of MAC₃₇₅ and k of the multi-VOC SOA were between the values of the two pure SOA.⁹ We therefore infer that the chromophores formed from phenol photooxidation under high-NO_x conditions were diluted by the nonabsorbing products from longifolene photooxidation.⁹ However, this dilution effect was not apparent when examining the multi-VOC SOA chemical composition.

In the phenol + longifolene system, similarities between $F_{C_2H_3O}$ and F_{CO_2} of the multi-VOC SOA and those of pure longifolene SOA suggest that the formation of both C₂H₃O⁺ and CO₂⁺ in the resulting SOA particles was influenced more significantly by the presence of longifolene instead of phenol, indicating an overall relatively low degree of oxidation of SOA. A very low fraction of ON was observed in the phenol + longifolene SOA, which is more consistent with the observation in the phenol SOA. Though the fraction of nitro-organics was more varied in the multi-VOC systems compared to single-VOC systems, we can still conclude that the $F_{N\text{-family}}$ in the phenol + longifolene experiments was between the $F_{N\text{-family}}$ from the two single-VOC systems. Based on these observations, it appears that either the formation of oxidized compounds from phenol + longifolene oxidation was mainly influenced by the longifolene oxidation pathway, which is reasonable since longifolene's reaction rate constant with OH[•] is higher than phenol's (4.70×10^{-11} vs 2.63×10^{-11} cm³/molecule/s),^{53,54} or as longifolene nucleated faster than phenol, it provided the surface for less oxygenated semi-volatile compounds to condense onto. However, in the presence of phenol, longifolene RO₂[•] was less likely to react with NO to form organonitrates because of the competition of phenol RO₂[•] reacting with NO, while the formation of nitro-organics was influenced by both VOCs. We conclude that the presence of oxidation products from two VOCs may have altered the original reaction pathways or created new reaction pathways that were not present in the single-VOC systems. For example, the RO₂[•] from the two VOCs may have reacted and formed an adduct, as further explained below.

The results of phenol + longifolene SOA from UPLC-DAD-ESI-HR-QTOFMS scanning first confirmed the presence of most compounds that were also present in samples from the single-VOC systems, and the main compounds that contributed to sample absorption were phenol related nitro-organics (Figure 3c and Table 2). There were two compounds for which we only observed their presence in the pure phenol system (C₁₃H₂₅NO₃ and C₁₁H₁₁NO₅), while in the multi-VOC system, their abundance was virtually undetectable at the corresponding retention times, indicating that with more radical species and potentially higher radical concentrations in the multi-VOC system, the oligomer formation process changed. We also confirmed the presence of some unique compounds in at least one of the analyzed multi-VOC samples that were not present in any single-VOC sample. These unique dimers, presumably formed from cross-reactions of phenol and longifolene higher generation oxidation products, include C₂₁H₃₁NO₅, C₂₁H₂₆N₃O₄, C₂₁H₂₈N₃O₇, C₂₀H₂₇NO₃, C₂₀H₂₅NO₄, C₂₀H₂₇NO₄, and C₁₉H₂₈N₃O₃. The presence of these dimers verified one of our hypotheses that with multiple VOCs in one system, their oxidation products led to new reactions that could not occur in the single-VOC systems. However, it is worth noting that the relative abundance of

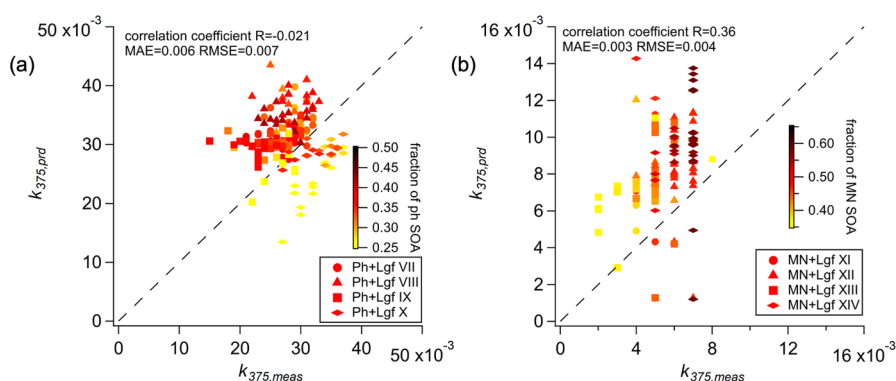


Figure 4. Predicted k ($k_{375,\text{prd}}$) vs measured k at 375 nm ($k_{375,\text{meas}}$) for (a) phenol + longifolene and (b) 1-methylnaphthalene + longifolene SOA particles. The dashed lines are 1:1 lines.

these dimers was much lower than that of the absorbing nitro-organic compounds. This observed difference in relative abundance could possibly be attributed to the low concentrations of these dimers formed in the experiments, the low electrospray ionization efficiencies of these dimers, or the chromatographic conditions that we used that were not optimized for retaining oligomers. Additionally, since the samples for UPLC-DAD-ESI-HR-QTOFMS were collected at the end of each experiment, we cannot infer the formation of these oligomers at earlier times in the experiments. Thus, with the current results, we are not able to evaluate their relative concentration or formation process.

3.2.2. 1-Methylnaphthalene + Longifolene System. Like the phenol + longifolene experiment results, the SOA particles from the 1-methylnaphthalene + longifolene experiments showed lower absorption than pure 1-methylnaphthalene SOA particles (1-methylnaphthalene + longifolene: $\text{SSA}_{375} = 0.98$, $\text{MAC}_{375} = 0.32 \text{ m}^2/\text{g}$, $k_{375} = 0.006$). As mentioned above, we believe the addition of longifolene, which mainly produced scattering compounds, diluted the absorbing molecules formed from 1-methylnaphthalene high- NO_x photooxidation; thus, the values of MAC_{375} and k of 1-methylnaphthalene + longifolene SOA were between the values of the two pure SOA.

1-Methylnaphthalene + longifolene SOA showed similar fractions of both $\text{C}_2\text{H}_3\text{O}^+$ and CO_2^+ ions to longifolene SOA, indicating that the presence of longifolene limited the formation of further oxidized products from 1-methylnaphthalene, or the fast nucleated longifolene SOA provided a surface for the condensation of less oxidized components. The observed contribution of ON to total SOA in the 1-methylnaphthalene + longifolene system was much lower than that of 1-methylnaphthalene SOA and closer to that of longifolene SOA. Additionally, like the phenol + longifolene system, the $F_{\text{N-family}}$ of 1-methylnaphthalene + longifolene SOA was between the $F_{\text{N-family}}$ of the two single-VOC SOA, indicating that a portion of the 1-methylnaphthalene RO_2^\bullet did not react with NO to form organonitrates as they did in the pure 1-methylnaphthalene system, while the formation of nitro-organics was controlled by both VOCs. Thus, we infer that the fate of some VOC oxidation products/intermediates has changed in this multi-VOC system compared to the single-VOC systems.

UPLC-DAD chromatogram of the 1-methylnaphthalene + longifolene SOA sample is shown in Figure 3d, which displays a highly similar elution pattern of absorbing compounds to that of the pure 1-methylnaphthalene SOA sample. The molecular

identification of major BrC chromophores confirmed that the main absorbing components were nitro-aromatics that were also present in the 1-methylnaphthalene sample (Table 2). However, different from the phenol + longifolene SOA sample, we did not identify any unique absorbing or non-absorbing oligomers in any 1-methylnaphthalene systems. Based on our results, oligomer formation had little to no influence on the chemical and optical properties of 1-methylnaphthalene + longifolene SOA.

3.3. Comparison between Measured and Predicted k in a Multi-VOC System. To better understand the absorption of SOA particles from the multi-VOC systems and evaluate if it can be quantitatively described by mixing of the SOA from individual VOCs, we first predicted the SOA k at 375 nm ($k_{375,\text{prd}}$) in multi-VOC systems using the results from a source apportionment model and the k_{375} of SOA from single-VOC systems and compared it with the measured k_{375} (Figure 4). Although we investigated the chemical composition of SOA particles from different systems using specific tracers, given the high fragmentation of samples in the mAMS, it is hard to determine the contribution of compounds from specific precursors to the total SOA by using only the tracers discussed above. Therefore, we used a source apportionment model to separate out the multi-VOC SOA organic mass spectrum and determine the fractional contribution of products from each VOC to the total SOA.

Organic mass spectra matrix from pure phenol, 1-methylnaphthalene, and longifolene were obtained from mAMS data during single-VOC oxidation experiments and used as inputs in the Positive Matrix Factorization (PMF)^{55,56} model with the Multilinear Engine algorithm (ME-2)^{57,58} along with the Source Finder (SoFi)³⁷ interface. The SOA from single-VOC experiments were apportioned into 1-2 factors based on the factor's mass spectral profile and time trend (an example is shown in Figure S13). Then we used PMF/ME-2-SoFi on mAMS data from the multi-VOC experiments to constrain the factors of the multi-VOC SOA with the known mass spectral profiles from aromatic and longifolene SOA (with an allowed variation of less than 10%), assuming the multi-VOC SOA was made of the compounds from single-VOC SOA only. Thus, the factors solved from multi-VOC SOA would include factors with mass spectral profiles of the known single-VOC SOA (an example is shown in Figure S14). Next, the fractional contribution from each factor to total SOA was calculated ($\text{Frac}_{\text{aromatic}}$ and $\text{Frac}_{\text{Lgfp}}$ shown in Figure S15) and used to determine $k_{375,\text{prd}}$ (Figure

SI6), which is the weighted, linear combination of single-VOC SOA k_{375} values (eq 5) based on the assumption that multi-VOC SOA was made of compounds that were the same as the compounds in the single-VOC systems.

For both phenol + longifolene and 1-methylnaphthalene + longifolene SOA, most of the $k_{375,\text{prd}}$ values were overestimated based on our linear combination assumption (Figure 4). The correlation coefficient (R), mean absolute error (MAE), and root mean square error (RMSE) of the predictions are low in both systems. For phenol + longifolene SOA, it is clear that $k_{375,\text{prd}}$ showed a dependence on the aromatic SOA fraction, while its $k_{375,\text{meas}}$ did not show such a dependence. For 1-methylnaphthalene + longifolene SOA, both $k_{375,\text{meas}}$ and $k_{375,\text{prd}}$ showed a dependence on the aromatic SOA content; however, $k_{375,\text{prd}}$ reached higher values than did $k_{375,\text{meas}}$. Therefore, k of the multi-VOC SOA cannot be accurately predicted by a linear combination assumption.

There are multiple potential reasons for the discrepancy between $k_{375,\text{prd}}$ and $k_{375,\text{meas}}$. First, the SOA chemical composition may not have been well described by PMF/ME-2-SoFi. Although aromatic and longifolene oxidation products had very different chemical and physical properties, due to the nature of mAMS, the mass spectra of these two types of compounds shared some similarity ($R^2 = 0.3\text{--}0.6$). This may lead to some uncertainty in the estimation of the SOA fractions. Note that the SoFi-resolved factors from the aromatic and longifolene systems were overall different from one another (Figure S17), indicating that despite a high degree of fragmentation, unique features based on the VOC backbone are preserved in the mass spectra of the corresponding SOA. Second, the linear combination assumption that is used to predict k cannot be applied to the multi-VOC systems as the unique oligomer formation might have more significant influence on SOA optical properties in the mixture system. With two types of VOCs in the system, the SOA growth might have been promoted because of the availability of a larger surface area, especially for phenol oxidation products, as longifolene oxidized and nucleated first, which could have provided enough surface area for semi-volatile phenol products to condense on. Alternatively, as the results from UPLC measurements showed, radicals from the two different VOCs could have gone through binary reactions that were different from those in the single-VOC experiments, leading to the formation of new compounds that had not been observed in the single-VOC experiments and inhibiting the formation of some other compounds. Such unique chemical components in the multi-VOC SOA could influence the $k_{375,\text{meas}}$ that we observed, depending on the molecule's chemical nature and optical properties, thus leading to the discrepancies between $k_{375,\text{prd}}$ and $k_{375,\text{meas}}$. Since the dimers in the multi-VOC system were potentially adducts of radicals from two different VOCs, once fragmented in the mAMS, the dimers would break down into ions that were highly similar to the ion fragments from the monomers, thus preventing PMF/ME-2 from identifying their presence as unique components.

In the second method, we estimated the fractions of SOA from each VOC based on the mass concentrations expected from each VOC considering their corresponding yield value. Predicted k values are presented in Table S11. Using these estimates of mass fractions results in better predictions of k for 1-methylnaphthalene + longifolene but not phenol + longifolene, confirming that a linear combination assumption

cannot be uniformly used to accurately predict the k of multi-VOC SOA.

4. ATMOSPHERIC IMPLICATIONS

This work provides important insights into the SOA and secondary BrC aerosol formation from single-VOC vs multi-VOC systems. Oxidation conditions in ambient atmosphere are better simulated by multi-VOC chamber experiments with a continuous flow of relevant oxidants than by single-VOC or batch experiments because the emissions of VOCs and other reactive species are continuous and mixed in the ambient environment. In this work, the continuous injections of NO in the chamber bag ensured that radicals predominantly reacted with NO or NO₂, favoring the formation of light-absorbing compounds. In fact, chemical simulations in the Master Chemical Mechanism (MCM) model indicated that because of our high NO_x conditions, 99% of the primary RO₂[•] radicals from phenol and longifolene oxidation reacted with NO. This dominating branching ratio pathway for RO₂[•] may not be common under typical ambient conditions. However, the resulting high NO_x conditions could be found in biomass burning emissions^{59,60} or polluted urban centers which are also important and complex sources of atmospheric BrC^{61–63} and a motivation for carrying out the current set of experiments. Thus, results from this work are critical to understanding the potential influence of VOC mixtures on SOA formation and properties under similar conditions.

The nonlinear effects from the presence of multiple VOCs on SOA chemical composition and absorption are expected to be important in environments where concentrations of reactive radicals are high. For example, during the daytime in urban areas, VOCs emitted from vehicles, other anthropogenic sources, urban greening, and the NO_x emitted from extensive traffic activities are mixed, resulting in conditions that are more complex than the photooxidation conditions in the experiments discussed above. As concluded above, with the presence of VOCs that have different reactivities with OH[•] and radical species from different precursors in one system, the chemical composition and absorption of the resulting SOA could not be well predicted simply by extrapolating values from single-VOC systems. However, the current models mostly simulate SOA formation and its properties by the oxidation of individual VOCs rather than treating the VOCs as a mixture and considering the multi-VOC's nonlinear interactive effects. This study indicates that this widely used simulation method has deficiencies, and thus could lead to disagreements between the simulated and observed aerosol concentrations and properties.^{64,65} In addition, since the extent of the nonlinear effects on SOA chemical composition and optical properties and the formation of oligomers between radicals from different precursors were found to vary in different systems, the different combinations of VOCs may result in different outcomes. Therefore, it is necessary to study the nonlinear effects on SOA formation and properties under different reaction regimes and more precursor combinations before drawing universal conclusions.

The absorption capacity of BrC is important to know, as it influences the outcome of aerosol total radiative forcing. The BrC radiative forcing modeling studies mainly include the BrC from biomass/biofuel burning OA,^{66,67} while some studies also include the contribution by aromatic SOA.^{6,68} Our study indicates that the absorption of aromatic SOA could change dramatically because of co-oxidation of other VOC species

(e.g., decrease in k from 0.074 in phenol SOA to 0.024 in phenol + longifolene SOA). This change in the observed SOA absorption property could potentially lead to disagreements between the simulated and measured BrC radiative forcing.⁶⁸ We recommend that future laboratory studies explore the nonlinear effects from oxidation of different combinations of VOCs, under different environmental conditions, on SOA formation and properties to improve our understanding of these effects. Furthermore, future aerosol radiative forcing simulation studies should include the multi-VOC nonlinear effect on secondary BrC formation and potentially on the aging of BrC.

■ ASSOCIATED CONTENT

SI Supporting Information

The Supporting Information is available free of charge at <https://pubs.acs.org/doi/10.1021/acsestair.3c00041>.

Details of online chemical characterization; Technical details of UPLC-DAD-ESI-HR-QTOFMS analysis; Details of the calculation of k_{425} ; Figure SI1: (a) SSA₃₇₅ vs aerosol mode diameter, (b) MAC₃₇₅ vs aerosol mode diameter, (c) time series of aerosol mode diameter, and (d) time series of n_{375} ; Figure SI2: SOA particle growth in each system; Figure SI3: ME-2/SoFi-resolved phenol SOA chemical composition; Figure SI4: ME-2/SoFi-resolved phenol + longifolene SOA chemical composition; Figure SI5: SoFi resolved fractional contribution from (a) longifolene factor, (b) phenol factor 1, (c) phenol factor 2 to organics in SOA in phenol + longifolene systems, (d) longifolene factor, (e) 1-methylnaphthalene factor 1, and (f) 1-methylnaphthalene factor 2 to organics in SOA in 1-methylnaphthalene + longifolene systems; Figure SI6: Time series of $k_{375,prd}$ in (a) phenol + longifolene, (b) 1-methylnaphthalene + longifolene experiments; Figure SI7: Normalized profile of longifolene factor vs (a) phenol factor 1 and (b) phenol factor 2; Table SI1: Predicted k based on yield calculations in multi-VOC experiments (PDF)

■ AUTHOR INFORMATION

Corresponding Author

Roya Bahreini – Department of Environmental Sciences, University of California, Riverside, Riverside, California 92521, United States; orcid.org/0000-0001-8292-5338; Email: roya.bahreini@ucr.edu

Authors

Yumeng Cui – Department of Environmental Sciences, University of California, Riverside, Riverside, California 92521, United States

Kunpeng Chen – Department of Environmental Sciences, University of California, Riverside, Riverside, California 92521, United States; orcid.org/0000-0002-9430-9257

Haofei Zhang – Department of Chemistry, University of California, Riverside, Riverside, California 92521, United States; orcid.org/0000-0002-7936-4493

Ying-Hsuan Lin – Department of Environmental Sciences, University of California, Riverside, Riverside, California 92521, United States; orcid.org/0000-0001-8904-1287

Complete contact information is available at: <https://pubs.acs.org/doi/10.1021/acsestair.3c00041>

Notes

The authors declare no competing financial interest.

■ ACKNOWLEDGMENTS

This work was supported by National Science Foundation (AGS 1454374), USDA NIFA Hatch Accession No. 1015963 (Project No. CA-R-ENS-5072-H). We thank Dr. Jie Zhou at the UC Riverside Analytical Chemistry Instrumentation Facility (ACIF) for the assistance with the UPLC-DAD-ESI-HR-QTOFMS (supported by NSF CHE-0541848). Y.C. gratefully acknowledge the support from UC Riverside Environmental Sciences Departmental Graduate Student Research Support, UC Riverside Sustainability Research Graduate Student Research Award, and UC Riverside Dissertation Year Fellowship.

■ REFERENCES

- (1) Bond, T.C.; Bergstrom, R.W. Light Absorption by Carbonaceous Particles: An Investigative Review. *Aerosol Science and Technology*. **2006**, *40* (1), 27–67.
- (2) Andreae, M.O.; Gelencsér, A. Black carbon or brown carbon? The nature of light-absorbing carbonaceous aerosols. *Atmos Chem. Phys.* **2006**, *6* (10), 3131–3148.
- (3) Laskin, A.; Laskin, J.; Nizkorodov, S.A. Chemistry of Atmospheric Brown Carbon. *Chem. Rev.* **2015**, *115* (10), 4335–4382.
- (4) Intergovernmental Panel on Climate Change. Anthropogenic and Natural Radiative Forcing. In *Climate Change 2013 - The Physical Science Basis*; Cambridge University Press: 2013; pp 659–740. DOI: [10.1017/CBO9781107415324.018](https://doi.org/10.1017/CBO9781107415324.018).
- (5) Feng, Y.; Ramanathan, V.; Kotamarthi, V.R. Brown carbon: A significant atmospheric absorber of solar radiation. *Atmos Chem. Phys.* **2013**, *13* (17), 8607–8621.
- (6) Wang, X.; Heald, C.L.; Liu, J.; et al. Exploring the observational constraints on the simulation of brown carbon. *Atmos Chem. Phys.* **2018**, *18* (2), 635–653.
- (7) Bellouin, N.; Quaas, J.; Gryspeerdt, E.; et al. Bounding Global Aerosol Radiative Forcing of Climate Change. *Reviews of Geophysics*. **2020**, *58* (1), No. e2019RG000660.
- (8) Zhang, A.; Wang, Y.; Zhang, Y.; et al. Modeling the global radiative effect of brown carbon: a potentially larger heating source in the tropical free troposphere than black carbon. *Atmos Chem. Phys.* **2020**, *20* (4), 1901–1920.
- (9) Liu, J.; Lin, P.; Laskin, A.; et al. Optical properties and aging of light-absorbing secondary organic aerosol. *Atmos Chem. Phys.* **2016**, *16* (19), 12815–12827.
- (10) Bluvshstein, N.; Lin, P.; Flores, J.M.; et al. Broadband optical properties of biomass-burning aerosol and identification of brown carbon chromophores. *Journal of Geophysical Research: Atmospheres*. **2017**, *122* (10), S441–S456.
- (11) Huang, R.J.; Yang, L.; Shen, J.; et al. Chromophoric Fingerprinting of Brown Carbon from Residential Biomass Burning. *Environ. Sci. Technol. Lett.* **2022**, *9* (2), 102–111.
- (12) He, Q.; Li, C.; Siemens, K.; et al. Optical Properties of Secondary Organic Aerosol Produced by Photooxidation of Naphthalene under NO_x Condition. *Environ. Sci. Technol.* **2022**, *56* (8), 4816–4827.
- (13) Nguyen, T.B.; Lee, P.B.; Updyke, K.M.; et al. Formation of nitrogen- and sulfur-containing light-absorbing compounds accelerated by evaporation of water from secondary organic aerosols. *Journal of Geophysical Research: Atmospheres*. **2012**, *117* (D1), No. D01207.
- (14) Cui, Y.; Frie, A.L.; Dingle, J.H.; et al. Influence of Ammonia and Relative Humidity on the Formation and Composition of Secondary Brown Carbon from Oxidation of 1-Methylnaphthalene and Longifolene. *ACS Earth Space Chem.* **2021**, *5* (4), 858–869.
- (15) Yang, Z.; Tsoma, N.T.; George, C.; Du, L. Nitrogen-Containing Compounds Enhance Light Absorption of Aromatic-Derived Brown Carbon. *Environ. Sci. Technol.* **2022**, *56* (7), 4005–4016.

- (16) Dingle, JH; Zimmerman, S.; Frie, AL; Min, J.; Jung, H.; Bahreini, R. Complex refractive index, single scattering albedo, and mass absorption coefficient of secondary organic aerosols generated from oxidation of biogenic and anthropogenic precursors. *Aerosol Science and Technology*. **2019**, *53* (4), 449–463.
- (17) Klodt, AL; Aiona, PK; MacMillan, AC; et al. Effect of relative humidity, NO_x and ammonia on the physical properties of naphthalene secondary organic aerosols. *Environmental Science: Atmospheres*. **2023**, *3* (6), 991–1007.
- (18) Baboosian, VJ; He, Q.; Montoya-Aguilera, J.; et al. Light absorption and scattering properties of indole secondary organic aerosol prepared under various oxidant and relative humidity conditions. *Aerosol Science and Technology*. **2023**, *57* (6), 532–545.
- (19) Yee, LD; Kautzman, KE; Loza, CL; et al. Secondary organic aerosol formation from biomass burning intermediates: Phenol and methoxyphenols. *Atmos Chem. Phys.* **2013**, *13* (16), 8019–8043.
- (20) Sato, K.; Takami, A.; Iozaki, T.; Hikida, T.; Shimono, A.; Imamura, T. Mass spectrometric study of secondary organic aerosol formed from the photo-oxidation of aromatic hydrocarbons. *Atmos Environ.* **2010**, *44* (8), 1080–1087.
- (21) Siemens, K.; Morales, A.; He, Q.; et al. Molecular Analysis of Secondary Brown Carbon Produced from the Photooxidation of Naphthalene. *Environ. Sci. Technol.* **2022**, *56* (6), 3340–3353.
- (22) Ng, N. L.; Chhabra, P. S.; Chan, A. W. H.; et al. Effect of NO_x level on secondary organic aerosol (SOA) formation from the photooxidation of terpenes. *Atmos Chem. Phys.* **2007**, *7* (19), 5159–5174.
- (23) Shilling, JE; Zaveri, RA; Fast, JD; et al. Enhanced SOA formation from mixed anthropogenic and biogenic emissions during the CARES campaign. *Atmos Chem. Phys.* **2013**, *13* (4), 2091–2113.
- (24) Zaveri, RA; Shilling, JE; Fast, JD; Springston, SR. Efficient Nighttime Biogenic SOA Formation in a Polluted Residual Layer. *Journal of Geophysical Research: Atmospheres*. **2020**, *125* (6), No. e2019JD031583.
- (25) Peng, Y.; Mouat, AP; Hu, Y.; Li, M.; McDonald, BC; Kaiser, J. Source apportionment of volatile organic compounds and evaluation of anthropogenic monoterpene emission estimates in Atlanta, Georgia. *Atmos Environ.* **2022**, *288*, No. 119324.
- (26) McFiggans, G.; Mentel, TF; Wildt, J.; et al. Secondary organic aerosol reduced by mixture of atmospheric vapours. *Nature*. **2019**, *565* (7741), 587–593.
- (27) Takeuchi, M.; Berkemeier, T.; Eris, G.; Ng, NL. Non-linear effects of secondary organic aerosol formation and properties in multi-precursor systems. *Nat. Commun.* **2022**, *13* (1), 7883.
- (28) Jiang, H.; Frie, AL; Lavi, A.; et al. Brown Carbon Formation from Nighttime Chemistry of Unsaturated Heterocyclic Volatile Organic Compounds. *Environ. Sci. Technol. Lett.* **2019**, *6* (3), 184–190.
- (29) Chen, K.; Raeofy, N.; Lum, M.; et al. Solvent effects on chemical composition and optical properties of extracted secondary brown carbon constituents. *Aerosol Science and Technology*. **2022**, *56* (10), 917–930.
- (30) Bohren, C. F.; Huffman, D. R. *Absorption and Scattering of Light by Small Particles*; Wiley, 1998. DOI: 10.1002/9783527618156.
- (31) Kim, H.; Paulson, SE. Real refractive indices and volatility of secondary organic aerosol generated from photooxidation and ozonolysis of limonene, α -pinene and toluene. *Atmos Chem. Phys.* **2013**, *13* (15), 7711–7723.
- (32) Saleh, R.; Hennigan, CJ; McMeeking, GR; et al. Absorptivity of brown carbon in fresh and photo-chemically aged biomass-burning emissions. *Atmos Chem. Phys.* **2013**, *13* (15), 7683–7693.
- (33) Frie, AL; Bahreini, R. Refractive index confidence explorer (RICE): A tool for propagating uncertainties through complex refractive index retrievals from aerosol particles. *Aerosol Science and Technology*. **2021**, *55* (6), 703–717.
- (34) Kroll, JH; Smith, JD; Che, DL; Kessler, SH; Worsnop, DR; Wilson, KR. Measurement of fragmentation and functionalization pathways in the heterogeneous oxidation of oxidized organic aerosol. *Physical Chemistry Chemical Physics*. **2009**, *11* (36), 8005.
- (35) Farmer, DK; Matsunaga, A.; Docherty, KS; et al. Response of an aerosol mass spectrometer to organonitrates and organosulfates and implications for atmospheric chemistry. *Proceedings of the National Academy of Sciences*. **2010**, *107* (15), 6670–6675.
- (36) Day, DA; Campuzano-Jost, P.; Nault, BA; et al. A systematic re-evaluation of methods for quantification of bulk particle-phase organic nitrates using real-time aerosol mass spectrometry. *Atmos Meas Technol.* **2022**, *15* (2), 459–483.
- (37) Canonaco, F.; Crippa, M.; Slowik, J. G.; Baltensperger, U.; Prévôt, A. S. H. SoFi, an IGOR-based interface for the efficient use of the generalized multilinear engine (ME-2) for the source apportionment: ME-2 application to aerosol mass spectrometer data. *Atmos Meas Technol.* **2013**, *6* (12), 3649–3661.
- (38) Lin, C.; Huang, RJ; Ceburnis, D.; et al. Extreme air pollution from residential solid fuel burning. *Nat. Sustain.* **2018**, *1* (9), 512–517.
- (39) Lin, C.; Ceburnis, D.; Trubetskaya, A.; et al. On the use of reference mass spectra for reducing uncertainty in source apportionment of solid-fuel burning in ambient organic aerosol. *Atmos Meas Technol.* **2021**, *14* (10), 6905–6916.
- (40) Borrás, E.; Tortajada-Genaro, LA. Secondary organic aerosol formation from the photo-oxidation of benzene. *Atmos Environ.* **2012**, *47*, 154–163.
- (41) Chan, A. W. H.; Kautzman, K. E.; Chhabra, P. S.; et al. Secondary organic aerosol formation from photooxidation of naphthalene and alkylnaphthalenes: implications for oxidation of intermediate volatility organic compounds (IVOCs). *Atmos Chem. Phys.* **2009**, *9* (9), 3049–3060.
- (42) Hettiyadura, A. P. S.; Garcia, V.; Li, C.; et al. Chemical composition and molecular-specific optical properties of atmospheric brown carbon associated with biomass burning. *Environ. Sci. Technol.* **2021**, *55* (4), 2511–2521.
- (43) Lin, P.; Bluvshstein, N.; Rudich, Y.; Nizkorodov, SA; Laskin, J.; Laskin, A. Molecular Chemistry of Atmospheric Brown Carbon Inferred from a Nationwide Biomass Burning Event. *Environ. Sci. Technol.* **2017**, *51* (20), 11561–11570.
- (44) Xie, M.; Chen, X.; Hays, MD; et al. Light Absorption of Secondary Organic Aerosol: Composition and Contribution of Nitroaromatic Compounds. *Environ. Sci. Technol.* **2017**, *51* (20), 11607–11616.
- (45) Yu, L.; Smith, J.; Laskin, A.; Anastasio, C.; Laskin, J.; Zhang, Q. Chemical characterization of SOA formed from aqueous-phase reactions of phenols with the triplet excited state of carbonyl and hydroxyl radical. *Atmos Chem. Phys.* **2014**, *14* (24), 13801–13816.
- (46) Gilardoni, S.; Massoli, P.; Paglione, M.; et al. Direct observation of aqueous secondary organic aerosol from biomass-burning emissions. *Proc. Natl. Acad. Sci. U. S. A.* **2016**, *113* (36), 10013–10018.
- (47) Mayorga, RJ; Zhao, Z.; Zhang, H. Formation of secondary organic aerosol from nitrate radical oxidation of phenolic VOCs: Implications for nitration mechanisms and brown carbon formation. *Atmos Environ.* **2021**, *244*, No. 117910.
- (48) Li, C.; He, Q.; Fang, Z.; et al. Laboratory Insights into the Diel Cycle of Optical and Chemical Transformations of Biomass Burning Brown Carbon Aerosols. *Environ. Sci. Technol.* **2020**, *54* (19), 11827–11837.
- (49) Zhang, X.; Lin, YH; Surratt, JD; Weber, RJ. Sources, Composition and Absorption Ångström Exponent of Light-absorbing Organic Components in Aerosol Extracts from the Los Angeles Basin. *Environ. Sci. Technol.* **2013**, *47* (8), 3685–3693.
- (50) Lin, P.; Liu, J.; Shilling, JE; Kathmann, SM; Laskin, J.; Laskin, A. Molecular characterization of brown carbon (BrC) chromophores in secondary organic aerosol generated from photo-oxidation of toluene. *Physical Chemistry Chemical Physics*. **2015**, *17* (36), 23312–23325.
- (51) Krueve, A.; Kaupmees, K.; Liigand, J.; Leito, I. Negative Electrospray Ionization via Deprotonation: Predicting the Ionization Efficiency. *Anal Chem.* **2014**, *86* (10), 4822–4830.

- (52) Laskin, J.; Laskin, A.; Nizkorodov, SA; et al. Molecular Selectivity of Brown Carbon Chromophores. *Environ. Sci. Technol.* **2014**, *48* (20), 12047–12055.
- (53) Atkinson, R.; Aschmann, SM; Arey, J. Reactions of hydroxyl and nitrogen trioxide radicals with phenol, cresols, and 2-nitrophenol at 296 ± 2 K. *Environ. Sci. Technol.* **1992**, *26* (7), 1397–1403.
- (54) Shu, Y.; Atkinson, R. Atmospheric lifetimes and fates of a series of sesquiterpenes. *J. Geophys. Res.* **1995**, *100* (D4), 7275–7281.
- (55) Paatero, P.; Tapper, U. Positive matrix factorization: A non-negative factor model with optimal utilization of error estimates of data values. *Environmetrics.* **1994**, *5* (2), 111–126.
- (56) Paatero, P. Least squares formulation of robust non-negative factor analysis. *Chemometrics and Intelligent Laboratory Systems.* **1997**, *37* (1), 23–35.
- (57) Paatero, P. The Multilinear Engine—A Table-Driven, Least Squares Program for Solving Multilinear Problems, Including the n-Way Parallel Factor Analysis Model. *Journal of Computational and Graphical Statistics.* **1999**, *8* (4), 854–888.
- (58) Paatero, P.; Hopke, PK. Rotational tools for factor analytic models. *J. Chemom.* **2009**, *23* (2), 91–100.
- (59) Trentmann, J.; Andreae, M. O.; Graf, H. Chemical processes in a young biomass-burning plume. *Journal of Geophysical Research: Atmospheres.* **2003**, *108* (D22), na DOI: 10.1029/2003JD003732.
- (60) Burling, I. R.; Yokelson, R. J.; Griffith, D. W. T.; et al. Laboratory measurements of trace gas emissions from biomass burning of fuel types from the southeastern and southwestern United States. *Atmos Chem. Phys.* **2010**, *10* (22), 11115–11130.
- (61) Yan, C.; Zheng, M.; Bosch, C.; et al. Important fossil source contribution to brown carbon in Beijing during winter. *Sci. Rep.* **2017**, *7* (1), 43182.
- (62) Xie, M.; Hays, MD; Holder, AL. Light-absorbing organic carbon from prescribed and laboratory biomass burning and gasoline vehicle emissions. *Sci. Rep.* **2017**, *7* (1), 7318.
- (63) Zhang, X.; Kim, H.; Parworth, CL; et al. Optical Properties of Wintertime Aerosols from Residential Wood Burning in Fresno, CA: Results from DISCOVER-AQ 2013. *Environ. Sci. Technol.* **2016**, *50* (4), 1681–1690.
- (64) Heald, C. L.; Coe, H.; Jimenez, J. L.; et al. Exploring the vertical profile of atmospheric organic aerosol: Comparing 17 aircraft field campaigns with a global model. *Atmos Chem. Phys.* **2011**, *11* (24), 12676–12696.
- (65) Reddington, CL; Morgan, WT; Darbyshire, E.; et al. Biomass burning aerosol over the Amazon: analysis of aircraft, surface and satellite observations using a global aerosol model. *Atmos Chem. Phys.* **2019**, *19* (14), 9125–9152.
- (66) Saleh, R.; Marks, M.; Heo, J.; Adams, PJ; Donahue, NM; Robinson, AL. Contribution of brown carbon and lensing to the direct radiative effect of carbonaceous aerosols from biomass and biofuel burning emissions. *Journal of Geophysical Research: Atmospheres.* **2015**, *120* (19), 10285–10296.
- (67) Brown, H.; Liu, X.; Feng, Y.; et al. Radiative effect and climate impacts of brown carbon with the Community Atmosphere Model (CAM5). *Atmos Chem. Phys.* **2018**, *18* (24), 17745–17768.
- (68) Jo, DS; Park, RJ; Lee, S.; Kim, SW; Zhang, X. A global simulation of brown carbon: implications for photochemistry and direct radiative effect. *Atmos Chem. Phys.* **2016**, *16* (5), 3413–3432.